Environmental Technology & Innovation 22 (2021) 101384

Contents lists available at ScienceDirect

Environmental Technology & Innovation

journal homepage: www.elsevier.com/locate/eti

Synthesis and study of functionalized magnetic graphene oxide for Pb^{2+} removal from wastewater

Maryam Zarenezhad [a], Mahmoud Zarei [a,*], Masoud Ebratkhahan [a], Mehdi Hosseinzadeh [b]

[a] Research Laboratory of Environmental Remediation, Department of Applied Chemistry, University of Tabriz, 51666-16471, Tabriz, Iran
[b] Marand Faculty of Technical and Engineering, University of Tabriz, 51666-16471, Tabriz, Iran

ARTICLE INFO

Article history:
Received 10 October 2020
Received in revised form 16 January 2021
Accepted 16 January 2021
Available online 19 January 2021

Keywords:
Adsorption
Functionalization
Magnetic graphene oxide
Lead ion

ABSTRACT

Heavy metals are among the environmental pollutants that human exposure to water and food can cause acute and dangerous poisoning. There are various methods for the removal of heavy metals. Among them, adsorption is considered to be an effective method for the removal of heavy metals. In this study, magnetic graphene oxide (MGO) nanocomposites functionalized with different amine ligands were used to remove Pb^{2+} from aqueous solutions. X-ray diffraction, Fourier-transform infrared spectroscopy, Scanning electron microscopy, Energy-dispersive X-ray spectroscopy and Vibrating-sample magnetometer analyzes were applied to determine the structure and characterization of the synthesized nanocomposites. Then, the factors affecting the adsorption efficiency such as pH, adsorbent amount, contact time and lead concentration were investigated and the optimum conditions for Pb^{2+} removal was the initial Pb^{2+} concentration of 20 mg/L, pH = 4, the adsorbent weight of 40 mg and the reaction time of 10 min. Pb^{2+} adsorption efficiency for adsorbents functionalized with ethylenediamine (EDA), melamine and monoethanolamine was compared. It was observed Pb^{2+} adsorption efficiency for these three adsorbents were 98%, 96.34% and 97.65%, respectively. Kinetic, isotherm and thermodynamic studies were also performed for the synthesized adsorbent and its recovery in the sequential adsorption and desorption cycle was investigated. The EDA functionalized MGO (EDA-MGO) adsorbent demonstrated 8.8% decrease in Pb^{2+} adsorption efficiency after 5 successive cycles of adsorption and desorption.

1. Introduction

In recent decades, the amount of human origin contaminants such as heavy metals have increased substantially in both surface and ground waters. The increase in water pollution has been considered as a grave danger for aqueous media and has led to the contamination of agricultural products. As a result, human health is severely threatened (Ngambia et al., 2019; Ramanayaka et al., 2019; Zhang et al., 2017).

All of the natural waters contain a variety of contaminants resulting from processes of erosion, washing, and weathering. In addition to these natural contaminants, other pollutants resulting from domestic wastewater and industrial wastewater are added. Water sources pollutants can be classified into different categories depending on the nature of

* Corresponding author.
E-mail addresses: s.maryam.zare@gmail.com (M. Zarenezhad), mzarei@tabrizu.ac.ir (M. Zarei), masoudebratkhahan@yahoo.com (M. Ebratkhahan), MH_1268@yahoo.com (M. Hosseinzadeh).

https://doi.org/10.1016/j.eti.2021.101384
2352-1864/

their origin. By nature of the contamination, water pollutants can be divided into three major groups of minerals (such as acidifying compounds, chemical fertilizers and heavy metals), biological (such as viruses, bacteria and parasites) and organic compounds (Khataee et al., 2019; Thomas and Langford, 2007; Zhou et al., 2019).

Heavy metals are considered as a severe threat to human beings due to their bioaccumulation, non-biodegradability and toxicity. Various toxic heavy metal ions are produced through several industrial activities, including electroplating, mining, radiator manufacturing, metal smelting, alloy industries, electrical and electronic industries, petrochemicals and electronics. These activities lead to an increase in the concentration of heavy metals in the environment and wastewater (Fernandes and Baeyens, 2019; Gu et al., 2015; Javanbakht and Ghoreishi, 2017; Rasoulpoor et al., 2020). Therefore, it is crucial to separate and to remove these heavy metals from wastewater and drinking water.

There are various methods for the removal of heavy metals such as ion exchange (Rae et al., 2019), coagulation (Cai et al., 2020), membrane processes (Azamat et al., 2020; Safarpour et al., 2016), polymers (Gómez-Ceballos et al., 2020), Zero-valent iron-based technologies (Wu et al., 2020a), electrochemical processes (Sun et al., 2020), and adsorption (Hernández-Cocoletzi et al., 2020). Most of these methods have disadvantages that limit their use. For example, ion exchange is confined to low concentrations of metallic solution where the membrane matrix is usually exposed to contamination with organic matter and other wastewater solids. This method has high initial investment and maintenance costs (Barakat, 2011). Coagulation and flocculation have high chemical consumption and increases the sludge production (Golob et al., 2005). The disadvantages of membrane processes are limited flow rate, membrane clogging, high initial investment cost, high maintenance and operating cost (Madaeni and Mansourpanah, 2003). Electrochemical processes have high operating costs (Kurniawan et al., 2006). Among these methods, adsorption is considered as an effective way to remove heavy metals from wastewater.

Adsorption is a cost-effective technology for removing heavy metals from the environment. Due to its high capacity, selectivity, low concentration efficiency, flexibility in operation, high efficiency and availability of a wide range of adsorbents, adsorption has attracted much attention (Chen et al., 2018; Demiral and Güngör, 2016). Therefore, the development of new and effective adsorbents to remove heavy metals has been one of the most active research efforts in wastewater treatment. Among various adsorbents, including silica gel, clays and zeolites, graphene-based materials are promising adsorbents for removing heavy metals due to their excellent electrical and mechanical properties (Chowdhury and Balasubramanian, 2014; de la Luz-Asunción et al., 2020). Carbon-based nanomaterials such as fullerenes (Yi et al., 2020), carbon nanotubes (CNTs) (Ali et al., 2019), activated carbon (Huang et al., 2020), graphene and graphene oxide (GO) (Lertcumfu et al., 2020; Wu et al., 2020b) have received much attention due to their excellent properties such as high surface area, adsorption capacity and selectivity in water treatment processes (Bethi et al., 2016; Khataee et al., 2013b; Wang et al., 2018). Graphene production methods are divided into two general categories. The first is methods in which graphite and its derivatives are used to produce graphene and the second is obtained without the use of graphite.

Graphene oxidation creates a new structure with different amounts of oxygen in its structure, depending on the oxidation conditions. Graphene oxide has outstanding charge carrier mobility and it can act as electron receivers and donors (Khataee et al., 2019; Motlagh et al., 2019). There are different oxygenated functional groups on the GO surface. These groups can be divided into two groups: the first group is functional groups on the surface of GO (such as hydroxyl and epoxide groups) and the second group is groups formed on the edge of GO (such as carboxylic acid and carbonyl groups) (Marcano et al., 2010). Graphene surface modification is necessary for many applications, since graphene may be ineffective in specific applications such as heavy metal ion adsorption (Cao and Li, 2014). As a result, the modification of GO through functional groups is ongoing research. Functional groups placed on magnetic GO, such as amine and carboxyl, have different chelating ability with heavy metal and toxic cations. Under the ambient pH conditions, functional groups can affect heavy cations and remove or reduce toxins from aquatic environments (Zhao et al., 2017a).

Advantages of this type of adsorbents include selective chelating power over specific metal cations, cation adsorption at very low concentrations of aqueous solutions, non-toxicity and metals recovery from aqueous media that can increase GO adsorption capacity for heavy metal ions (Gul et al., 2016). When GO becomes magnetic, its magnetic properties make it easy and fast to separate the adsorbent and provides reusability of adsorbent (Geng et al., 2012). Binding of magnetic particles to the GO surface can enhance the absorption capacity of GO and facilitate process efficiency (Yang et al., 2009).

The overall goal of this project is to investigate the ability of functionalized magnetic GO nanoparticles to adsorb Pb^{2+}. GO is synthesized via improved Hummers method. Afterward, it is magnetized and functionalized. X-ray diffraction (XRD) analysis, Fourier transform infrared spectroscopy (FT-IR), scanning electron microscopy (SEM) and Vibrating-sample magnetometer (VSM) are applied to investigate the properties of the resulting nanostructures. The effect of parameters such as adsorbent weight, pH, time and Pb^{2+} initial concentration on the process will also be investigated via experimental design. The isoelectric pH, isotherm, kinetics and thermodynamics of the synthesized adsorbent will also be investigated.

2. Materials and methods

2.1. Chemicals

Ethanol 96% (Kimia Alcohol Zanjan, Iran), potassium permanganate 99% (Merck, Germany), sulfuric acid 98% (Merck, Germany), sodium hydroxide 99% (Merck, Germany), graphite (Merck, Germany), phosphoric acid 35% (Merck, Germany), hydrochloric acid 35% (Merck, Germany), iron (III) chloride hexahydrate (Merck, Germany), sodium nitrate (Merck,

Germany), lead (II) nitrate 99.5% (Merck, Germany), ethylenediamine ≥99% (EDA, Merck, Germany), ethylene glycol ≥99.5% (Merck, Germany), melamine 99% (Merck, Germany), monoethanolamine (MEA, Merck, Germany), acetic acid 96% (Merck, Germany) and sodium acetate ≥99% (Merck, Germany) were supplied in this research. All chemicals were consumed without further purification.

2.2. Characterization and instruments

Philler magnetic stirrer (Taiwan), 86502 Az pH meter (Taiwan), MIRA3 FEG-SEM Tescan (Czech Republic), Bruker FT-IR Tensor 27 model (Germany), Philips PW1730 XRD device (the Netherlands), Hermle Labortechnik centrifuge Z 36 HK model (Germany–Denmark), Furat electronics shaker-incubator machine BS630 model (Iran), Analytik Jena atomic absorption machine Nova AA 400 model (Germany) and MDFK Meghnatis daneshpazhouh Kashan VSM apparatus (Iran) were applied in current study for adsorbent preparation and characterization.

2.3. Synthesis of functionalized magnetic graphene oxide

For the synthesis of GO from graphite, there are three standard methods known as the Hummers method, the modified Hummers method and the improved Hummers method. In this research, the improved Hummers method was used and the most significant difference with the two previous methods is the use of phosphoric acid instead of sodium nitrate. For the synthesis of GO by the improved Hummers method, 1 g of graphite was stirred continuously at room temperature for 18 h with 120 ml of sulfuric acid and 14 ml of phosphoric acid. It must be noted that the volumetric ratio of sulfuric acid/phosphoric acid must be 9:1 in this method. After 18 h, 6 g of potassium permanganate was added slowly as an oxidizing agent to the acidic graphite solution. The reaction temperature should be about 20 °C. Afterward; the resulting solution was stirred continuously at 50 °C for 12 h. Next, a solution containing 300 ml of deionized water and 10 ml of oxygenated water solution was prepared. Then, the solution containing graphite was slowly added to this solution. It must be noted that the last step takes place in the ice bath. The resulting solution was remained the same until its sediments were settled and it was washed with hydrochloric acid and deionized water for several times to achieve neutral pH. The resulting solution was placed in an ultrasonic bath for 20 min and immersed in a freeze dryer to produce powdered GO (Alkhouzaam et al., 2020; Guerrero-Contreras and Caballero-Briones, 2015).

For the preparation of magnetic graphene oxide (MGO), the prepared GO was dispersed in ethylene glycol by improved Hummers method. Then, this solution was stirred by adding sodium acetate and iron (III) chloride hexahydrate to the mixture at 30 °C. The solution temperature was kept at above 190 °C to form black sediments. Afterward, the sediments were filtered and washed with distilled water and ethanol and dried in an oven.

Later the resulted MGO was mixed with diluted acetic acid (12% V/V). Subsequently, the EDA was added and dissolved in ethylene glycol to form MGO functionalized with EDA (EDA-MGO). After stirring at 60 °C, the mixture was washed with ethanol and water and separated with a magnet. Finally, the nanoparticles were dried in the oven (Zhao et al., 2017b).

For functionalization of GO with melamine, 0.2 g of GO was poured into 35 ml of ethylene glycol and it was sonicated for 3 h. Next, 0.7 g of iron (III) chloride hexahydrate, 4.5 g of melamine and 1.4 g of sodium acetate was added to GO dissolved in ethylene glycol and the solution was sonicated for half an hour at 50 °C. The prepared solution is placed in a Teflon-coated autoclave at 200 °C for 6 h. The resulted precipitate by the reaction is removed from the solution by a magnet due to its magnetic properties. To remove impurities from the sediment, it was washed with deionized water and ethanol and dried at 45 °C (Hao et al., 2010) and the MGO functionalized with melamine (M-MGO) was obtained.

For GO functionalization with MEA to form MGO functionalized with MEA (MEA-MGO), the same steps of functionalization with melamine were repeated, except that instead of melamine, MEA was added to the solution. In this study, EDA, melamine and MEA were used as ligands to activate MGO.

2.4. Calculating adsorption efficiency

In this research, adsorption efficiency (AE) was applied to analyze the results. AE represents the amount of adsorbed Pb^{2+} as follows (Eq. (1)):

$$AE\% = \frac{(C_0 - C)}{C_0} \times 100 \tag{1}$$

where C_0 represents the initial Pb^{2+} concentration of the solution, C represents the concentration of Pb^{2+} solution after adsorption according to the atomic absorption results and AE represents the adsorption efficiency during specific adsorption times.

Table 1
Variables levels for Pb^{2+} removal.

Variables	Parameters and levels				
	−2	−1	0	1	2
$[Pb^{2+}]_0$ (mg/L) (X_1)	5	10	15	20	25
pH (X_2)	2	4	6	8	10
Adsorbent weight (mg) (X_3)	10	20	30	40	50
Time (min) (X_4)	5	10	15	20	25

2.5. Optimization of the adsorption process via response surface methodology

In this project, the central composite design (CCD) method was used to optimize the adsorption process to remove Pb^{2+}. The number of experiments will vary according to the number of parameters in this method. To evaluate the effect of operating parameters on the Pb^{2+} removal process and modeling, four main factors include initial Pb^{2+} concentration (mg/L), initial solution pH, reaction time (min) and adsorbent weight (mg) were evaluated (Table 1). Then, Minitab16 software designed the experiment based on these four factors and 31 experiments were recommended by the software. The following polynomial second-order equation was used to correlate between dependent and non-dependent variables (Eq. (2)):

$$Y = \beta_0 + \sum_{i=1}^{k} \beta_i X_i + \sum_{i=1}^{k} \beta_{ii} X_i^2 + \sum_{1 \le i \le j}^{k} \beta_{ij} X_i X_j \tag{2}$$

where Y is the response variable (adsorption efficiency), X_i and X_j are the experimental levels of variables, β_i is the linear correlation coefficient, β_{ii} is the second-order correlation coefficient, b_{ij} is the cross-correlation coefficient and i, j and k are the number of variables (Arsalani et al., 2018; Khataee et al., 2013a, 2010).

3. Results and discussion

3.1. Characterization

Fig. 1 illustrates the FT-IR spectra of EDA-MGO, M-MGO and MEA-MGO. As can be seen, since all three synthesized MGOs were functionalized with substances having amine functional groups, there is a little difference in their IR spectra. For this reason, the interpretation of these three spectrums was done together. According to the figures, the peak at 3250 cm^{-1} represents the hydroxyl functional groups (O–H) and the peak at 3391 cm^{-1} represents the amine (N–H) functional groups. The peaks of 2829 cm^{-1} and 2914 cm^{-1} represent the C–H bonds, indicating the formation of carbon shell on the adsorbent. Other common peaks observed in the graphene structure are C=O peaks, which appear in the spectrum of 1697 cm^{-1}. The absorbance peak at the 1398 cm^{-1} region corresponds to the C–N bond on the adsorbent surface. The absorption peak in the range of 530 cm^{-1} corresponds to the Fe–O bond in the magnetic iron nanoparticles, which indicates the coating of magnetic iron nanoparticles with the carbon. The presence of C–O bonds at 1431 cm^{-1} and C=C at 1552 cm^{-1} also indicates the correct structure of synthesized GO (Cao et al., 2015; Guo et al., 2013).

Fig. 2 shows the XRD patterns of GO, MGO, EDA-MGO, M-MGO and MEA-MGO. The peak present at 2θ of 11.2° is attributed to the synthesized GO (Verma et al., 2020; Wang et al., 2016). The peaks at 2θ of 34.3°, 43.2°, 57.5° and 63.2° represent the (0 2 2), (1 1 3), (0 0 4), (2 2 4), (1 2 5) and (0 4 4) sheets which corresponded to Fe_3O_4, indicating that GO has been successfully magnetized (Huang et al., 2018; Wang et al., 2016). It is also observed that with the magnetization of GO, its peak intensity in EDA-MGO and MEA-MGO was increased at $2\theta = 36°$. For EDA, the peaks at 28.2°, 34.3°, 43.2°, 57.5° and 63.2° were observed. For melamine, the peaks at 27.2°, 33.3° and 44.2° and for MEA, the peaks at 24.2°, 34.8°, 38.2°, 48.5° and 63.2° were observed.

Fig. 3a displays the SEM images of GO which is confirmed the layered structure of synthesized GO. Fig. 3b shows the SEM image of the synthesized MGO. As can be seen, the iron particles are present on the surface of GO layers, which means the GO was successfully magnetized. This was in accordance with the dot mapping results of the MGO (Fig. SM-2b). Fig. 3c displays the SEM images of EDA-MGO. It is observed that with the functionalization of MGO, the prominence and roughness of MGO layers increased and the EDA functional groups were unevenly distributed on the surface. Fig. 3d demonstrates the SEM images of M-MGO. It is observed that, like EDA functionalization, in the M-MGO, the prominence and surface area of M-MGO was increased. The amine functional groups were unevenly distributed on the surface and the layered form of the surface was preserved. Fig. 3e shows the SEM images of MEA-MGO. It is observed, MEA-MGO's surface is also layered and the surface prominence of GO is lower than the EDA-MGO and M-MGO. Fig. 3f demonstrates the SEM images of EDA-MGO after the Pb^{2+} adsorption process. It is observed that by the adsorption of lead via EDA-MGO, the bulk density and accumulation of Pb^{2+} particles on the surface are increased and the particles are stacked together. The adsorbent particle size was also increased a little with the functionalization and the adsorption of Pb^{2+}. It was observed that the average layer thickness of GO was about 30 nm and the average particle size of GO was increased from 18.44 nm

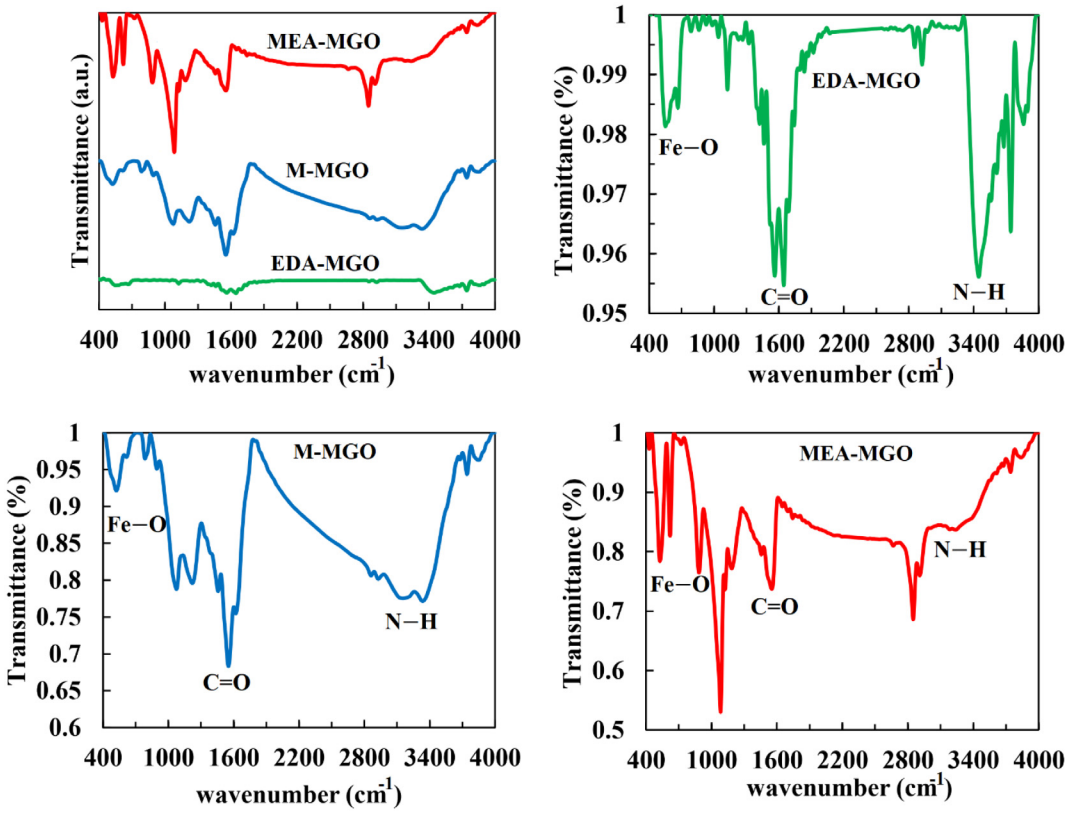

Fig. 1. FT-IR spectra of EDA-MGO, M-MGO and MEA-MGO.

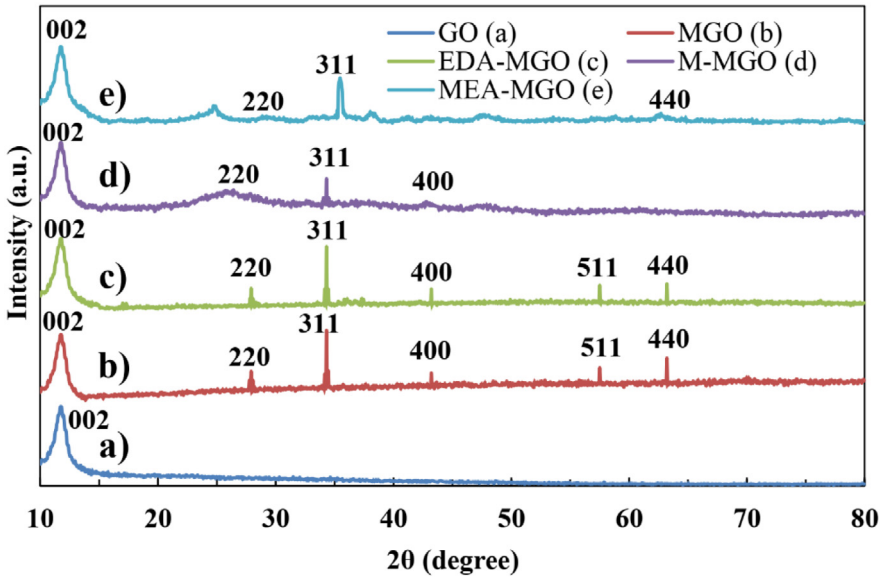

Fig. 2. XRD patterns of (a) GO, (b) MGO, MGO functionalized with (c) EDA, (d) melamine and (e) MEA.

after magnetization to 28.90 nm after functionalization with EDA, to 23.90 nm after functionalization with melamine, to 23.50 nm after functionalization with EDA and finally to 35.02 nm after adsorption of Pb^{2+} by EDA-MGO.

EDX and dot mapping analysis was applied to prove the presence of iron and amine on the adsorbent surface and investigate the distribution of the elements on the adsorbent surface. The results are shown in Figs. SM-1 and SM-2 and

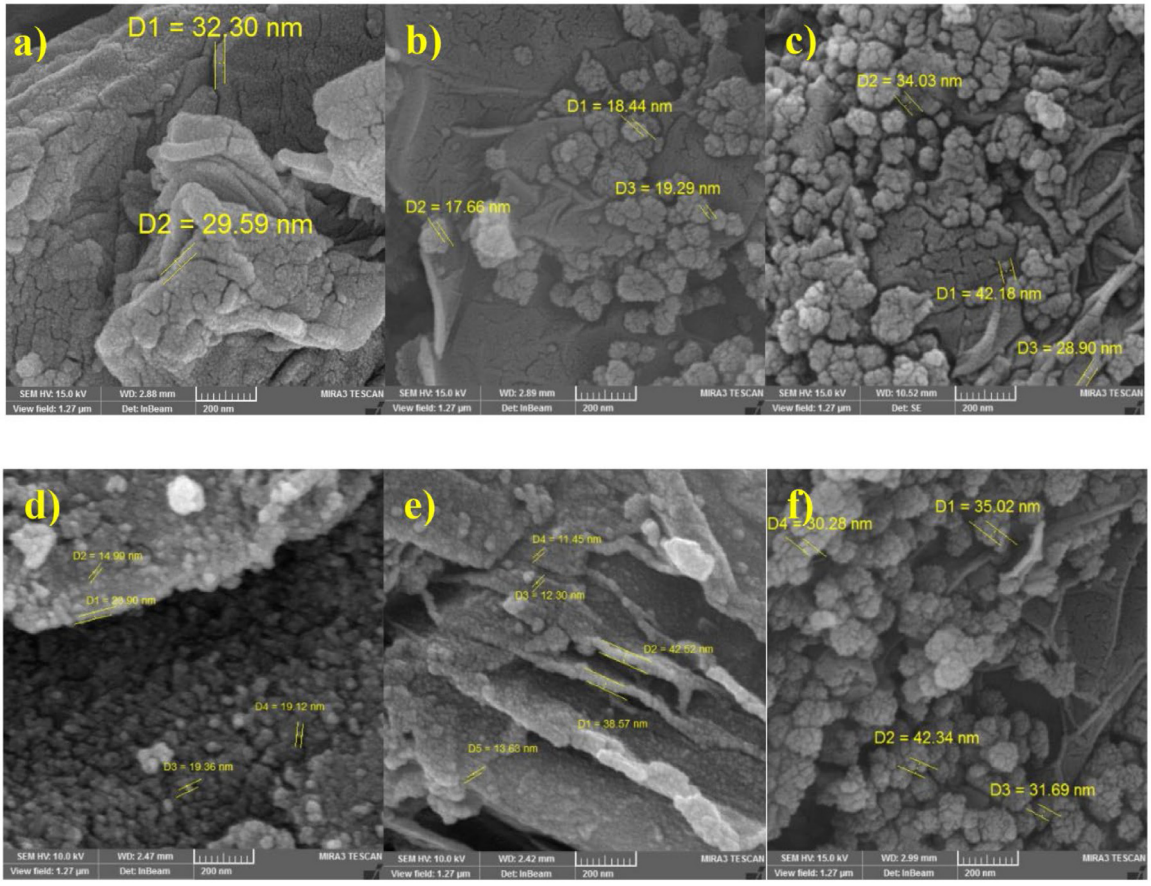

Fig. 3. SEM images of: (a) GO, (b) MGO, (c) EDA-MGO, (d) M-MGO, (e) MEA-MGO before Pb^{2+} absorption and (f) EDA-MGO after Pb^{2+} adsorption.

Table SM-1, according to the weight percentage of elements at the GO structure. Carbon (C), oxygen (O), iron (Fe), nitrogen (N) and lead (Pb) are found in the investigated structure. The Fe amount indicates the presence of iron in the adsorbent, which means GO adsorbent was magnetized. The presence of N indicating the functionalization of the adsorbent with the amine functional group and the presence of Pb shows the adsorption of Pb on the EDA functionalized adsorbent.

The EDX and dot mapping results of MGO illustrates the presence of C, O and Fe in the MGO structure, indicating that the GO was first magnetized. Carbon is mainly present in GO nanostructures and oxygen is found in GO functional groups. Iron is also found in the structure due to the magnetization of GO. The EDX and dot mapping results of EDA-MGO, M-MGO and MEA-MGO show the presence of O, C, Fe and N in the GO structure. The weight percentage results of each adsorbent indicate that in the second stage MGOs are functionalized with EDA, melamine and MEA due to the presence of nitrogen in the adsorbent structure. The EDX and dot mapping result of Pb-EDA-MGO shows that O, C, Fe, N and Pb are present in the compound structure. The presence of lead in the structure also indicates the removal and absorption of lead by the adsorbent.

The magnetic behavior change of the EDA-MGO adsorbent was compared with pure Fe_3O_4 using the hysteresis loops recorded by VSM (Fig. SM-3 and Table SM-2). The minor *SQR* values out of S-shaped hysteresis loop that is the signature figure of the superparamagnetic materials. As expected, the magnetization amount of the EDA-MGO adsorbent decreased to 25.47 emu/g. Nonetheless, the magnetism of the samples was strong enough for their facile separation (Fig. SM-4).

3.2. Analysis of variance

Using Minitab 16 software and based on the results, the following correlation coefficients and the following second-order equation between response variable and independent variables were obtained:

$$Y = 21.5819 + 1.04568X_1 - 2.85283X_2 + 1.20901X_3 + 4.99015X_4 - 0.23971X_1X_2 + 0.04160X_1X_3 - 0.03848X_1X_4 - 0.17534X_2X_3 + 0.23358X_2X_4 - 0.02441X_3X_4 - 0.08376X_1^2 - 0.57334X_2^2 - 0.00740X_3^2 - 0.15601X_4^2 \quad (3)$$

Table 2
Experimental and RSM predicted results for Pb^{2+} adsorption.

Run	$[Pb^{2+}]_0$ (mg/L)	pH	Adsorbent weight (mg)	Time (min)	Adsorption efficiency (%)	
					Experimental	Predicted
1	20	4	20	20	85.00	85.16
2	25	6	30	15	93.00	92.40
3	10	4	20	10	86.00	85.91
4	15	6	30	15	93.75	94.36
5	15	6	30	15	94.00	94.36
6	15	6	30	15	95.40	94.36
7	15	6	30	15	94.55	94.36
8	20	8	20	10	83.80	83.68
9	15	6	30	15	94.50	94.36
10	15	6	10	15	92.00	91.99
11	15	6	30	25	83.40	82.77
12	20	4	40	20	89.00	89.43
13	20	8	20	20	92.20	92.88
14	20	8	40	20	86.50	87.00
15	15	6	30	15	94.60	94.36
16	20	4	40	20	93.00	94.36
17	15	6	30	15	94.70	94.36
18	15	6	50	15	91.42	90.80
19	20	4	40	10	98.00	98.32
20	10	4	40	10	91.00	90.61
21	20	8	40	10	82.00	82.68
22	20	4	20	10	85.00	85.30
23	10	4	20	20	90.00	89.62
24	5	6	30	15	79.00	79.56
25	15	10	30	15	77.00	76.43
26	15	2	30	15	94.00	93.94
27	20	4	20	20	85.00	85.16
28	25	6	30	15	93.00	92.40
29	10	4	20	10	86.00	85.91
30	15	6	30	15	93.75	94.36
31	15	6	30	15	94.00	94.36

Table 3
ANOVA analysis of Pb^{2+} adsorption.

Source variations	Sum of squares	Degree of freedom	Adjusted of Mean square	F-value
Regression	845.329	19	44.491	211.51
Residuals	2.314	11	0.210	
Total	847.643	30		

It should be noted that the above equation is uncoded. Table 2 shows the experimental results and the results based on the Eq. (3). According to the results, it can be concluded this model can accurately model the experimental results and can be used to predict the output variable under different conditions.

Statistical analysis of variance (ANOVA) is commonly applied to test the significance and appropriateness of the obtained model. Table 3 shows the results of the ANOVA. The correlation coefficient (R^2) obtained from this method is 99.23%, which is a good and acceptable value and indicates how much variability in the response variable can be explained by experimental factors and their interactions. The obtained value also indicates that 99.23% of the variability in Pb^{2+} adsorption efficiency can be justified by independent variables and the model cannot be justified for 0.27% of the variation. Comparison of the experimental results of the Pb^{2+} adsorption efficiency with the results of the response surface methodology (RSM) is shown in Fig. 4, which is well overlapped (99.2%).

3.2.1. The effect of pH and Pb^{2+} concentration on adsorption efficiency and isoelectric point determination

Figs. 5 and 6a show the isoelectric point graph, two-dimensional and three-dimensional graphs of the effect of pH and Pb^{2+} concentration on the adsorption efficiency of EDA-MGO adsorbent with 30 mg adsorbent and duration of 15 min. As can be seen, by increasing the pH until about 6 and increasing the concentration of lead until about 20 mg/L, the adsorption efficiency will increase. After passing through these points, the adsorption efficiency will decrease. The pH value of the solution plays an important role in the whole process and the adsorption capacity (Ifthikar et al., 2020). It affects not only the surface charge of the adsorbent but also the ionization degree of the substances available in the solution. It also affects the separation of the functional groups in the active sites of the adsorbent and solution. Therefore, electrostatic attraction between the adsorbent and the heavy metal is pH-dependent and in this process, pH of up to 6 is favorable.

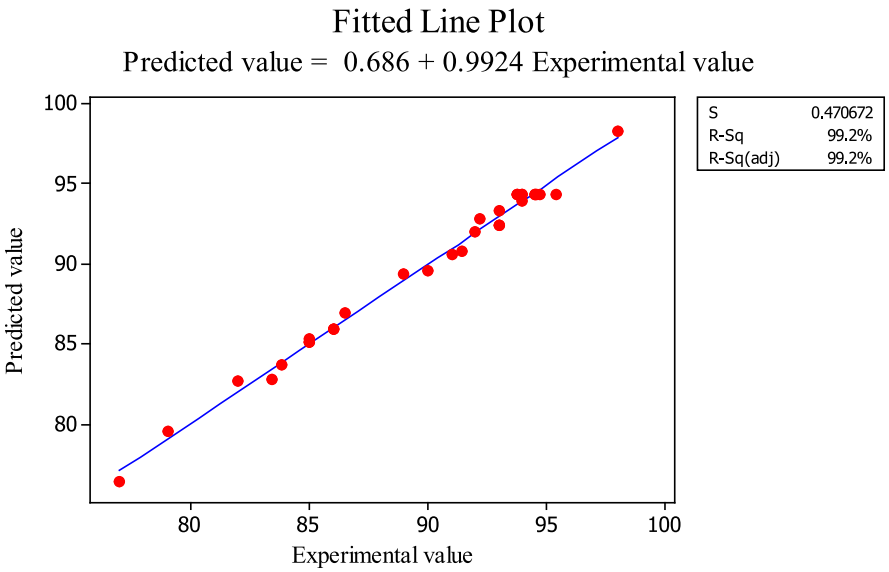

Fig. 4. Comparison of experimental results of adsorption efficiency with the predicted results of the RSM.

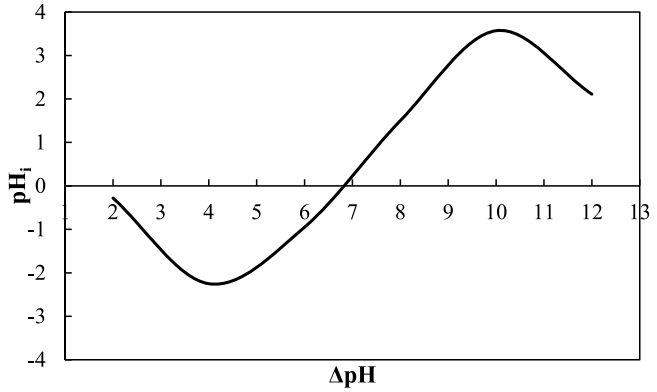

Fig. 5. Isoelectric point diagram of EDA-MGO.

This could be described by the fact that at low pH, a high concentration of H^+ could react with amine groups to form protonation and Pb^{2+} uptake is decreased consequently. In other words, H^+ could compete with Pb^{2+} ions for adsorption sites on the copolymer and reduce the metal ions adsorption capacity. At higher pH values (higher than 3), the nitrogen of primary amine group on the adsorbent was completely deprotonated, so Pb^{2+} uptake was intense and the reactive sites of the adsorbent could be occupied with Pb^{2+} ions. At pH values higher than 6, the adsorption efficiency value of Pb^{2+} was decreased a little and adsorption process occurs simultaneously with the precipitation of metal hydroxide (Hosseinzadeh, 2018; Mahmoud et al., 2010).

For the isoelectric point test, six 0.1 N sodium nitrate solutions were prepared and the pH of the solutions was adjusted to 2, 4, 6, 8, 10 and 12 by hydrochloric acid and sodium hydroxide. Each of these solutions contained 40 mg of the adsorbent. Then, all of the samples were stirred for 2 days. After 2 days, the pH of the solutions was re-measured and pH_i and ΔpH were collected (Fig. 5). According to the isoelectric point graph, it was found that the isoelectric point pH is about 6.8. It was observed that at acidic pH, the adsorbent surface charge is negative and at the basic pH, the adsorbent surface charge is positive. Considering the Pb^{2+} charge, acidic pH is favorable to create electrostatic attraction between the adsorbent and the heavy metal, which is consistent with our findings through experimental design.

3.2.2. The effect of adsorbent weight and pb^{2+} concentration on adsorption efficiency

Fig. 6b shows two-dimensional and three-dimensional graphs of the effect of adsorbent weight and Pb^{2+} concentration on adsorption efficiency for a solution with pH = 6 and reaction time of 15 min. As can be seen, as the adsorbent weight

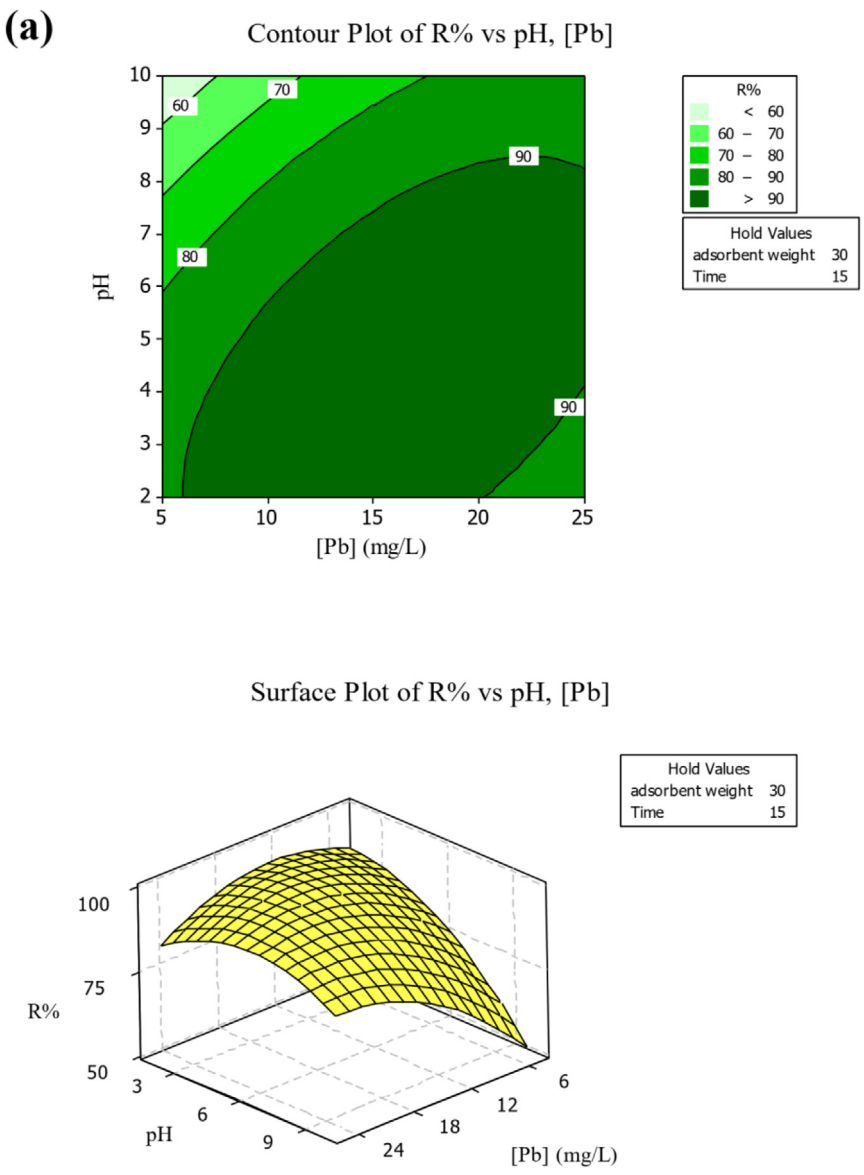

Fig. 6. Two and three-dimensional diagrams of (a) the effect of pH and Pb^{2+} concentration, (b) the effect of adsorbent weight and Pb^{2+} concentration and (c) the effect of adsorption time and adsorbent weight on adsorption efficiency.

increases, the adsorption efficiency increases. As the concentration of lead decreases, the adsorption efficiency decreases. The adsorbent amount is another important factor since it determines the amount of pollutant removal. The reason for the increase in adsorption efficiency is partly related to the flow fission phenomenon (difference of concentration between the adsorbent and the adsorbed material), which means that the adsorption phenomena occurs rapidly on the adsorbent at higher concentrations. This results in a decrease in the concentration of adsorbed material in the solution compared to the lower concentration of the adsorbent (Alpat et al., 2008; Wang and Ariyanto, 2007).

3.2.3. The effect of time and adsorbent weight on adsorption efficiency

Fig. 6c shows two-dimensional and three-dimensional diagrams of the effect of time and adsorbent weight on adsorption efficiency for a solution with pH = 6 and lead concentration of 15 mg/L. It can be seen from the graphs that the adsorption efficiency at different weights increases slightly with the increase of the adsorbent weight due to the increase in the adsorbent surface. Usually, the adsorption increases by the time passing. After passing the optimum adsorption time in this experiment (14–20 min), the adsorption efficiency will be decreased slightly at each of the experimented adsorbent weights.

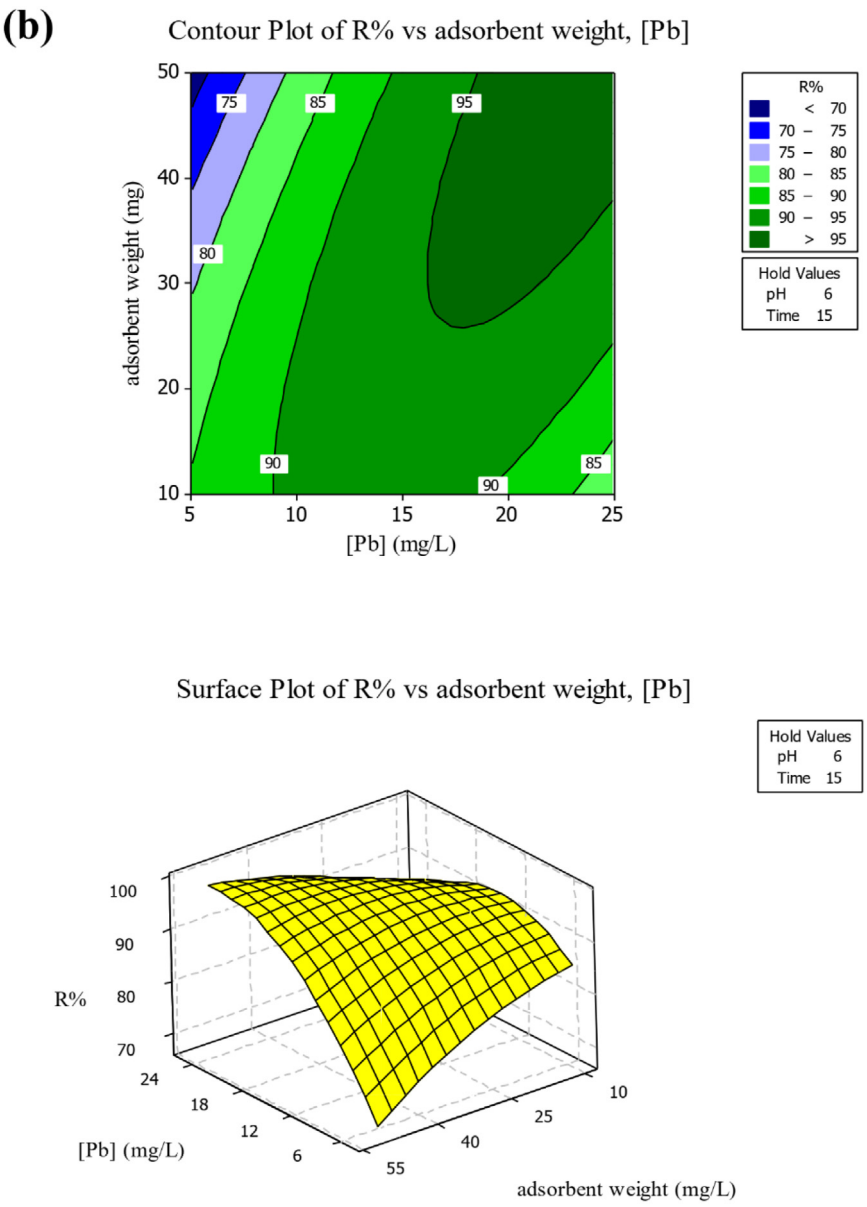

Fig. 6. (*continued*).

3.2.4. Determination of optimum Pb^{2+} removal conditions

The optimum way to eliminate Pb^{2+} is to achieve maximum adsorption efficiency. Therefore, optimal test conditions were determined via Minitab 16 software (Table 4). According to the obtained results, the optimum conditions for the Pb^{2+} removal are the initial Pb^{2+} concentration of 20 mg/L, pH = 4, the adsorbent weight of 40 mg and process time of 10 min. The maximum Pb^{2+} adsorption efficiency at these conditions was 98.32%. After obtaining the optimum conditions, an experiment was performed in these conditions and the results showed a good agreement between the experimental value (98%) and the predicted value (98.32%) of the model. This demonstrates the success of applying the RSM in optimizing the adsorption process.

3.3. Comparison of MGO functionalized with EDA, melamine and MEA and comparison with literatures

To investigate the Pb^{2+} removal values by M-MGO and MEA-MGO adsorbents, Pb^{2+} removal experiments were performed in optimum conditions and the obtained values for EDA-MGO, M-MGO and MEA-MGO adsorbents were compared. It was observed that Pb^{2+} adsorption efficiency for EDA-MGO, M-MGO and MEA-MGO were 98.00%, 96.34%

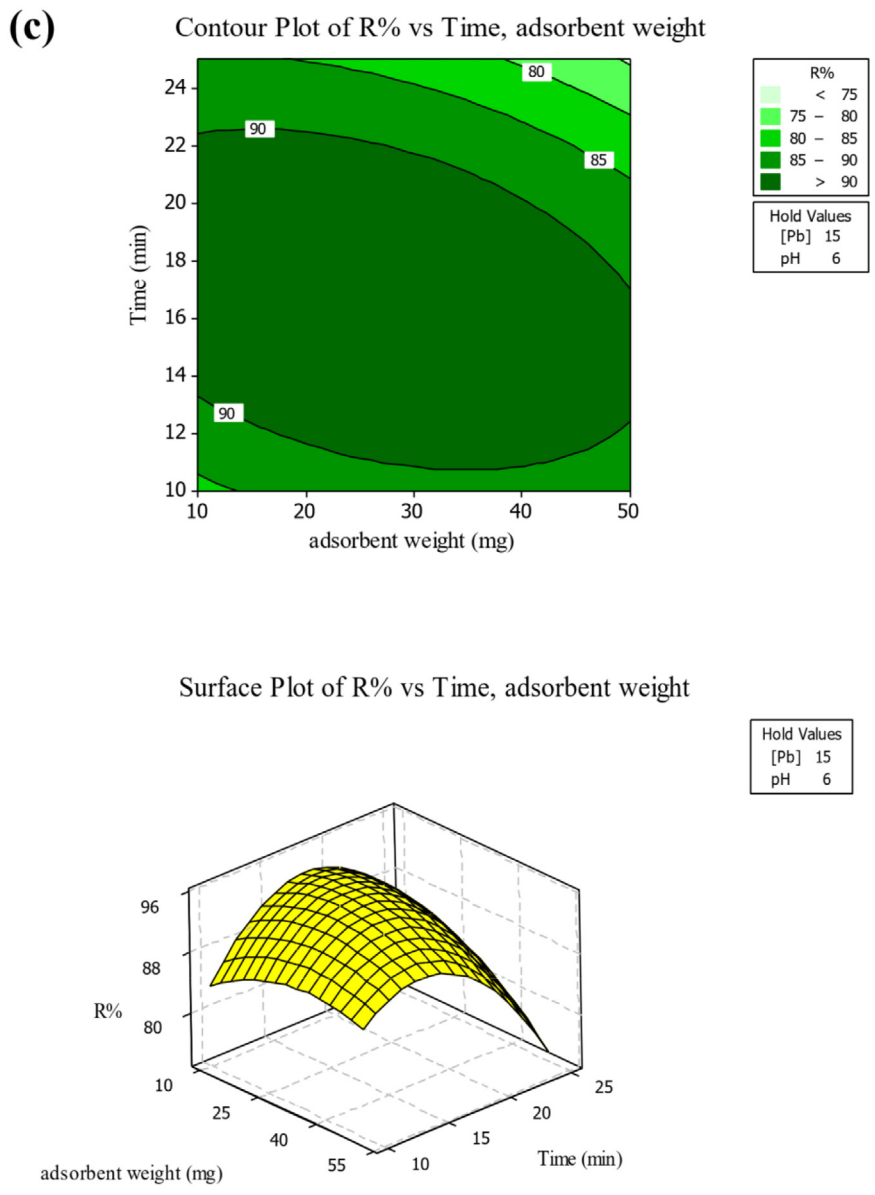

Fig. 6. (*continued*).

Table 4
Optimal amounts of operational parameters for maximum Pb^{2+} adsorption efficiency.

Variables	Optimum amount
$[Pb^{2+}]_0$ (mg/L) (X_1)	20
pH (X_2)	4
Adsorbent weight (mg) (X_3)	40
Time (min) (X_4)	10
Predicted adsorption efficiency	98.32
Experimental adsorption efficiency	98.00

and 97.65%, respectively. The observed difference in Pb^{2+} adsorption efficiencies is negligible and the obtained values are approximately the same. Therefore, considering these quantities and economic issues, EDA-MGO was selected as the optimum adsorbent at this process. It is also considered the reason for lower Pb^{2+} adsorption efficiency of the M-MGO

Table 5
Comparison of adsorption capacity of adsorbents for Pb^{2+} adsorption.

Adsorbent	Adsorption capacity (mg/g)	Ref.
Magnetic chitosan	47.91	Wang et al. (2016)
MnO_2-modified graphite	92.35	Zhao et al. (2017a)
MnO_2/CNTs	78.74	Ma et al. (2007)
Magnetic activated carbon	253.20	Zhang et al. (2020)
Porous lignin xanthate resin	64.90	Li et al. (2015)
Sultone-modified MAC[b]	147.05	Nejadshafiee and Islami (2019)
ACPAH[a]	21.80	Rao et al. (2009)
Fe_3O_4	166.67	Tamez et al. (2016)
Schleichera oleosa bark	69.40	Khatoon et al. (2018)
EDA-MGO	425.83	This study

[a]Activated carbon prepared from *Phaseolus aureus* hulls.
[b]Magnetic activated carbon.

Table 6
Investigation of thermodynamic parameters.

T (°C)	$\Delta G°$ (KJ/mol)	$\Delta H°$ (KJ/mol)	$\Delta S°$ (KJ/mol)
25	−11.0046	2366.66	44.87
45	−11.9020		

adsorbent compared to the other two adsorbents is the bulkiness of melamine and the creation of a space barrier (Afsar et al., 2020).

The adsorption capacity of the synthesized EDA-MGO adsorbent was compared with literatures. As can be seen at Table 5, the results are inspiring comparing the obtained data for Pb^{2+} adsorption via various adsorbents. The high adsorption capacity of EDA-MGO adsorbent due to its high surface area and layered structure could be very helpful at removing heavy metals such as Pb^{2+} and the adsorbent can be easily separated via its magnetic properties.

3.4. Investigation of adsorption isotherms, reaction kinetics and thermodynamic parameters of the adsorption process

The Langmuir, Freundlich and Temkin isotherms graphs were plotted and analyzed (Fig. 7a–c and Tables SM-3-5). It was observed that the data have the highest overlap amount with the Langmuir isotherm. Therefore, the adsorption process on the applied EDA functionalized graphene adsorbent is carried out in a layered manner (Zhao et al., 2017a).

To investigate the reaction kinetics, Pb^{2+} solution with an initial concentration of 20 mg/L and adsorbent weight of 40 mg at pH = 4 was prepared and stirred at ambience temperature. The solutions were sampled at 1, 2, 3, 5, 7, 10, 13, 17, 21 and 25 min and the kinetic data and graphs of the first-order, second-order and permeation models were plotted (Fig. 8a–c and Table SM-6). By comparing the obtained correlation coefficient values, it was found that the kinetics of the adsorption reaction follows the second-order type.

For thermodynamic studies, solutions with concentrations of 20 mg/L at temperatures of 25 °C and 45 °C at 1 to 25 min intervals were applied (Şimşek et al., 2017). By Eqs. (4)–(6), the ΔS and ΔH values of the reaction were calculated:

$$K_C = \frac{C}{C_i - C} \tag{4}$$

$$lnK_C = \frac{\Delta S}{R} - \frac{\Delta H}{RT} \tag{5}$$

$$\Delta G = \Delta H - T\Delta S \tag{6}$$

In the mentioned equations, c_i is the initial concentration, c is the concentration at the specified times and K_c is the thermodynamic constant at the specified temperature (25 °C and 45 °C). The results are presented in Table 6. As we know, thermodynamics is the study of physical and chemical changes and the temperature dependence of the adsorption process provides essential information on some thermodynamic parameters such as enthalpy, entropy and Gibbs free energy. The positive ΔH value indicates that the adsorption process is endothermic and confirms the strong chemical force between the metal and the adsorbent molecules, which indicates the chemical adsorption (Şimşek et al., 2017; Zhao et al., 2017a). The positive ΔS value of the adsorption process in this system will cause the disorder on the solid/soluble surface. The negative ΔG value is also a reason for the spontaneous adsorption process.

3.5. Process reusability check

To ensure the reusability of the Pb^{2+} adsorption process, the efficiency of Pb^{2+} adsorption was tested in 5 consecutive cycles using 0.5 M HCl solution at the optimum point (Zhao et al., 2017a). It was observed the adsorption efficiency after

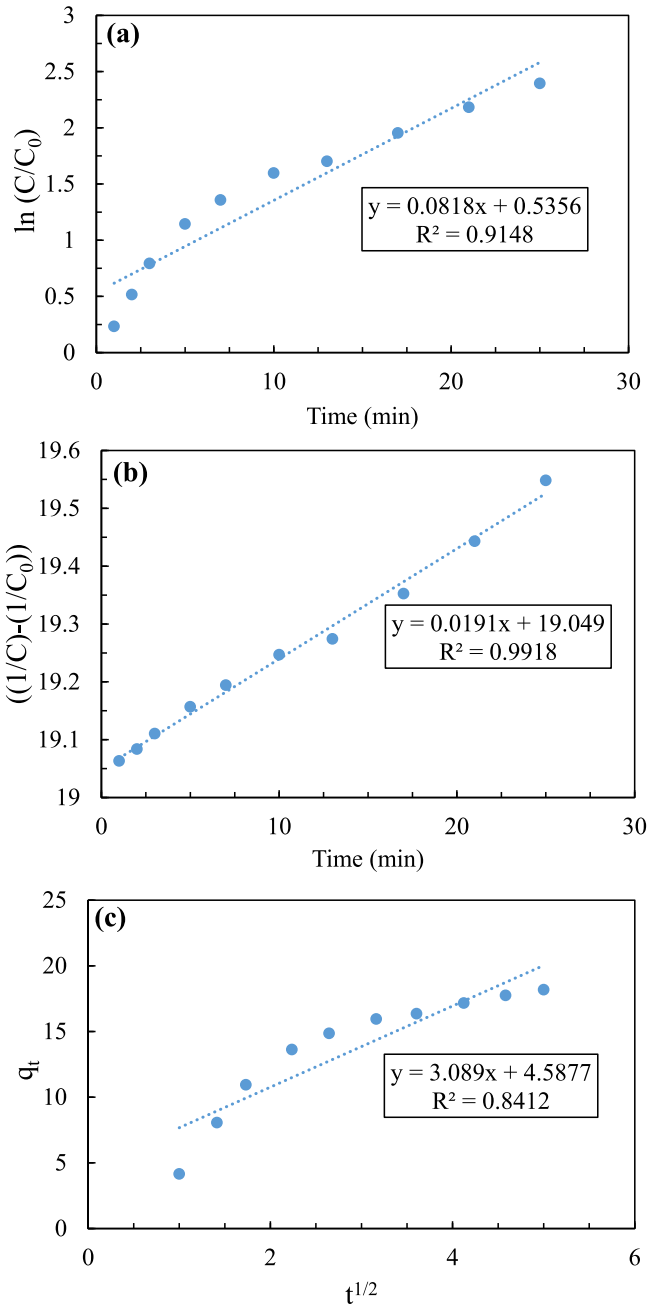

Fig. 7. (a) First-order, (b) second-order and (c) permeation model kinetic diagrams.

5 cycles was decreased about 8.8% from 98% to 89.2% (Fig. 9), which indicates that the adsorption process is reliable and with acceptable efficiency (Zavareh et al., 2015). It also shows that the EDA-MGO adsorbent can be easily regenerated via treatment with Pb^{2+} solution and has high durability.

4. Conclusion

In this study, MGO nanocomposites functionalized with EDA, melamine and MEA were applied to remove Pb^{2+} from aqueous solutions. For this purpose, the improved Hummers method was used for the synthesis of GO. Then, the synthesized GO was magnetized and finally was functionalized with EDA, melamine and MEA. The XRD, FT-IR, SEM and EDX analyzes were applied to determine the structure and characterization of the synthesized nanocomposites. The results

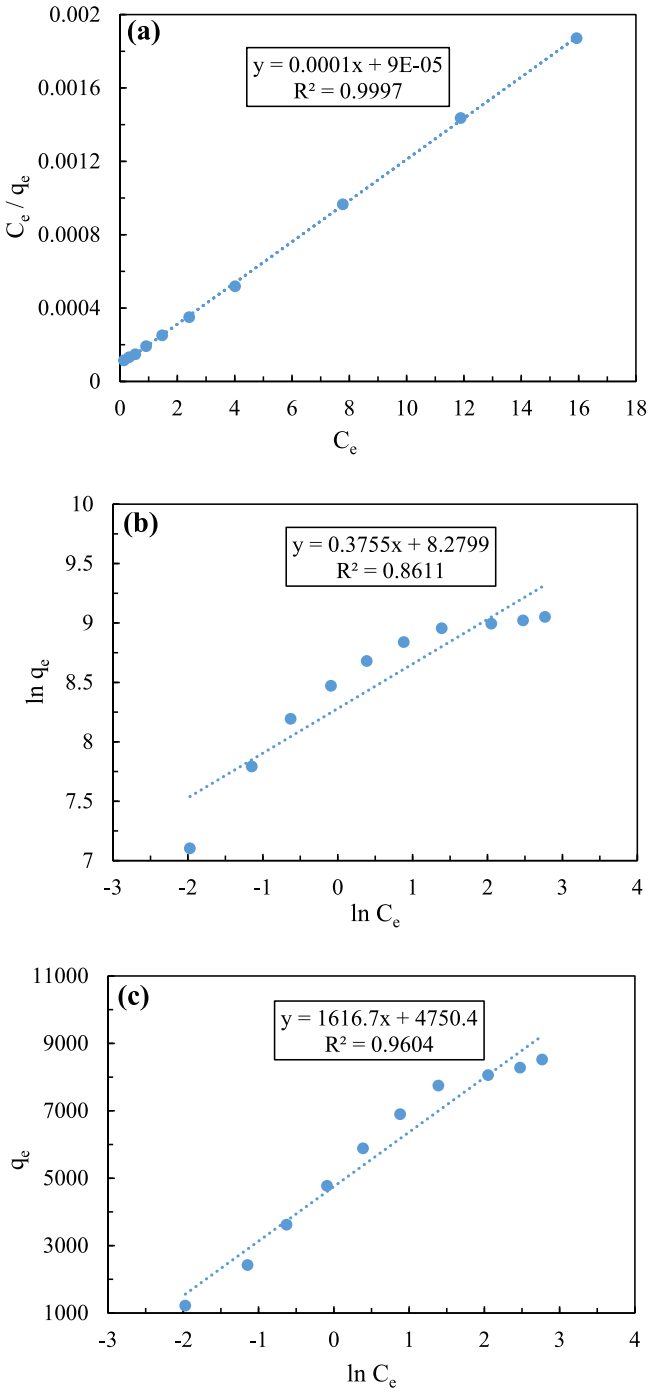

Fig. 8. (a) Langmuir, (b) Freundlich and (c) Temkin isothermal diagrams.

confirmed that GO synthesis processes, magnetization and functionalization were successfully performed. Next, the factors affecting the adsorption efficiency such as pH, adsorbent amount, contact time and initial concentration of Pb^{2+} were investigated and the optimum conditions for removal were obtained. At the initial Pb^{2+} concentration of 20 mg/L, pH = 4, the adsorbent weight is 40 mg and the reaction time is 10 min; about 98% of Pb^{2+} removal was observed. Comparing the experimental results of the Pb^{2+} adsorption efficiency with the RSM model results exhibited that the results of the experimental section and the model have good overlap (99.2%).

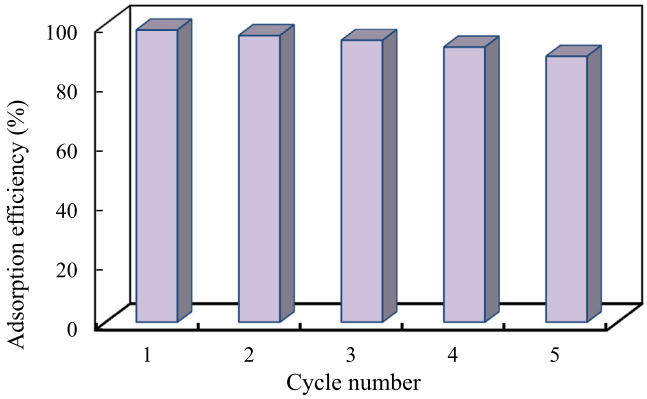

Fig. 9. Adsorbent reusability diagram over 5 cycles.

The Pb^{2+} adsorption efficiency for EDA-MGO, M-MGO and MEA-MGO adsorbents was compared and it was observed that Pb^{2+} adsorption efficiency for these three adsorbents were 98%, 96.34% and 97.65%, respectively. Therefore, the EDA-MGO adsorbent had the highest adsorption and was considered as the optimum adsorbent. Kinetic and isotherm studies were performed for EDA-MGO adsorbent and it was observed that the adsorption process follows the second-order kinetics and Langmuir isotherm. Thermodynamic parameters were investigated and the process was found to be spontaneous and endothermic. Also, the adsorption repeatability of the EDA-MGO was evaluated in 5 successive cycles of adsorption and desorption and the adsorbent demonstrated 8.8% decrease in Pb^{2+} adsorption efficiency, which is acceptable. According to studies, the synthesis reaction of magnetized graphene oxide with each of the melamine and MEA ligands has not been reported in journals. The study of the adsorption behavior of the adsorbents named with Pb^{2+} has been done for the first time in this research work. The results of this study presented that this method is an excellent technique to remove Pb^{2+} from wastewater containing this metal.

CRediT authorship contribution statement

Maryam Zarenezhad: Investigation. **Mahmoud Zarei:** Supervision. **Masoud Ebratkhahan:** Writing - review & editing. **Mehdi Hosseinzadeh:** Visualization.

Declaration of competing interest

The authors declare that they have no known competing financial interests or personal relationships that could have appeared to influence the work reported in this paper.

Acknowledgment

The authors would like to thank the University of Tabriz, Iran for the provided support.

Appendix A. Supplementary data

Supplementary material related to this article can be found online at https://doi.org/10.1016/j.eti.2021.101384.

References

Afsar, J., Zolfigol, M.A., Khazaei, A., Zarei, M., Gu, Y., Alonso, D.A., Khoshnood, A., 2020. Synthesis and application of melamine-based nano catalyst with phosphonic acid tags in the synthesis of (3'-indolyl) pyrazolo [3, 4-b] pyridines via vinylogous anomeric based oxidation. Mol. Catal. 482, 110666.

Ali, S., Shah, I.A., Ahmad, A., Nawab, J., Huang, H., 2019. Ar/O_2 plasma treatment of carbon nanotube membranes for enhanced removal of zinc from water and wastewater: A dynamic sorption-filtration process. Sci. Total Environ. 655, 1270–1278.

Alkhouzaam, A., Qiblawey, H., Khraisheh, M., Atieh, M., Al-Ghouti, M., 2020. Synthesis of graphene oxides particle of high oxidation degree using a modified Hummers method. Ceram. Int..

Alpat, S.K., Özbayrak, Ö., Alpat, Ş., Akçay, H., 2008. The adsorption kinetics and removal of cationic dye, Toluidine Blue O, from aqueous solution with Turkish zeolite. J. Hazard. Mater. 151 (1), 213–220.

Arsalani, N., Nasiri, R., Zarei, M., 2018. Synthesis of magnetic 3D graphene decorated with $CaCO_3$ for anionic azo dye removal from aqueous solution: Kinetic and RSM modeling approach. Chem. Eng. Res. Des. 136, 795–805.

Azamat, J., Sardroodi, J.J., Poursoltani, L., Jahanshahi, D., 2020. Functionalized boron nitride nanosheet as a membrane for removal of Pb^{2+} and Cd^{2+} ions from aqueous solution. J. Molecular Liquids 114920.

Barakat, M., 2011. New trends in removing heavy metals from industrial wastewater. Arab. J. Chem. 4 (4), 361–377.
Bethi, B., Sonawane, S.H., Bhanvase, B.A., Gumfekar, S.P., 2016. Nanomaterials-based advanced oxidation processes for wastewater treatment: a review. Chem. Eng. Process.-Process Intensif. 109, 178–189.
Cai, L., Sun, J., Cui, L., Jiang, Y., Huang, Z., 2020. Stabilization of heavy metals in piggery wastewater sludge through coagulation-hydrothermal reaction–pyrolysis process and sludge biochar for tylosin removal. J. Cleaner Prod. 121165.
Cao, Y., Li, X., 2014. Adsorption of graphene for the removal of inorganic pollutants in water purification: a review. Adsorption 20 (5–6), 713–727.
Cao, L., Yin, S., Liang, Y., Zhu, J., Fang, C., Chen, Z., 2015. Preparation and characterisation of magnetic Fe_3O_4/graphene oxide nanocomposites. Mater. Res. Innov. 19 (sup1), S1-364-S361-368.
Chen, H., Luo, J., Wang, X., Liang, X., Zhao, Y., Yang, C., Baikenov, M.I., Su, X., 2018. Synthesis of Al_2O_3/carbon composites from wastewater as superior adsorbents for Pb (II) and Cd (II) removal. Microporous Mesop. Mater. 255, 69–75.
Chowdhury, S., Balasubramanian, R., 2014. Recent advances in the use of graphene-family nanoadsorbents for removal of toxic pollutants from wastewater. Adv. Colloid Interface Sci. 204, 35–56.
Şimşek, S., Şenol, Z.M., Ulusoy, H.I., 2017. Synthesis and characterization of a composite polymeric material including chelating agent for adsorption of uranyl ions. J. Hazard. Mater. 338, 437–446.
de la Luz-Asunción, M., Perez-Ramirez, E.E., Martinez-Hernandez, A.L., García-Casillas, P.E., Luna-Bárcenas, J.G., Velasco-Santos, C., 2020. Adsorption and kinetic study of reactive red 2 dye onto graphene oxides and graphene quantum dots. Diam. Relat. Mater. 108002.
Demiral, H., Güngör, C., 2016. Adsorption of copper (II) from aqueous solutions on activated carbon prepared from grape bagasse. J. Cleaner Prod. 124, 103–113.
Fernandes, M.M., Baeyens, B., 2019. Cation exchange and surface complexation of lead on montmorillonite and illite including competitive adsorption effects. Appl. Geochem. 100, 190–202.
Geng, Z., Lin, Y., Yu, X., Shen, Q., Ma, L., Li, Z., Pan, N., Wang, X., 2012. Highly efficient dye adsorption and removal: a functional hybrid of reduced graphene oxide–Fe_3O_4 nanoparticles as an easily regenerative adsorbent. J. Mater. Chem. 22 (8), 3527–3535.
Golob, V., Vinder, A., Simonič, M., 2005. Efficiency of the coagulation/flocculation method for the treatment of dyebath effluents. Dyes Pigment. 67 (2), 93–97.
Gómez-Ceballos, V., García-Córdoba, A., Zapata-Benabithe, Z., Velásquez, J., Quintana, G., 2020. Preparation of hyperbranched polymers from oxidized lignin modified with triazine for removal of heavy metals. Polym. Degrad. Stab. 179, 109271.
Gu, X., Yang, Y., Hu, Y., Hu, M., Wang, C., 2015. Fabrication of graphene-based xerogels for removal of heavy metal ions and capacitive deionization. ACS Sustain. Chem. Eng. 3 (6), 1056–1065.
Guerrero-Contreras, J., Caballero-Briones, F., 2015. Graphene oxide powders with different oxidation degree, prepared by synthesis variations of the Hummers method. Mater. Chem. Phys. 153, 209–220.
Gul, K., Sohni, S., Waqar, M., Ahmad, F., Norulaini, N.N., A.K., M.O, 2016. Functionalization of magnetic chitosan with graphene oxide for removal of cationic and anionic dyes from aqueous solution. Carbohydr. Polymers 152, 520–531.
Guo, S., Zhang, G., Guo, Y., Jimmy, C.Y., 2013. Graphene oxide–Fe_2O_3 hybrid material as highly efficient heterogeneous catalyst for degradation of organic contaminants. Carbon 60, 437–444.
Hao, Y.-M., Man, C., Hu, Z.-B., 2010. Effective removal of Cu (II) ions from aqueous solution by amino-functionalized magnetic nanoparticles. J. Hazard. Mater. 184 (1–3), 392–399.
Hernández-Cocoletzi, H., Salinas, R.A., Águila Almanza, E., Rubio-Rosas, E., Chai, W.S., Chew, K.W., Mariscal-Hernández, C., Show, P.L., 2020. Natural hydroxyapatite from fishbone waste for the rapid adsorption of heavy metals of aqueous effluent. Environ. Technol. Innov. 20, 101109.
Hosseinzadeh, M., 2018. Removal of heavy metal ions from aqueous solutions using modified poly (styrene-alt-maleic anhydride) copolymer as a chelating resin. Russ. J. Appl. Chem. 91 (12), 1984–1993.
Huang, Q., Chen, Y., Yu, H., Yan, L., Zhang, J., Wang, B., Du, B., Xing, L., 2018. Magnetic graphene oxide/MgAl-layered double hydroxide nanocomposite: one-pot solvothermal synthesis, adsorption performance and mechanisms for Pb^{2+}, Cd^{2+}, and Cu^{2+}. Chem. Eng. J. 341, 1–9.
Huang, X., Wan, Y., Shi, B., Shi, J., 2020. Effects of powdered activated carbon on the coagulation-flocculation process in humic acid and humic acid-kaolin water treatment. Chemosphere 238, 124637.
Ifthikar, J., Shahib, I.I., Sellaoui, L., Jawad, A., Zhao, M., Chen, Z., Chen, Z., 2020. pH tunable anionic and cationic heavy metal reduction coupled adsorption by thiol cross-linked composite: Physicochemical interpretations and fixed-bed column mathematical model study. Chem. Eng. J. 401, 126041.
Javanbakht, V., Ghoreishi, S.M., 2017. Application of response surface methodology for optimization of lead removal from an aqueous solution by a novel superparamagnetic nanocomposite. Adsorp. Sci. Technol. 35 (1–2), 241–260.
Khataee, A., Alidokht, L., Hassani, A., Karaca, S., 2013a. Response surface analysis of removal of a textile dye by a Turkish coal powder. Adv. Environ. Res. 2 (4), 291–308.
Khataee, A., Marandizadeh, H., Vahid, B., Zarei, M., Joo, S.W., 2013b. Combination of photocatalytic and photoelectro-Fenton/citrate processes for dye degradation using immobilized N-doped Tio_2 nanoparticles and a cathode with carbon nanotubes: central composite design optimization. Chem. Eng. Process.: Process Intensif. 73, 103–110.
Khataee, A., Rad, T.S., Nikzat, S., Hassani, A., Aslan, M.H., Kobya, M., Demirbaş, E., 2019. Fabrication of NiFe layered double hydroxide/reduced graphene oxide (NiFe-LDH/rGO) nanocomposite with enhanced sonophotocatalytic activity for the degradation of moxifloxacin. Chem. Eng. J. 375, 122102.
Khataee, A.R., Zarei, M., Moradkhannejhad, L., 2010. Application of response surface methodology for optimization of azo dye removal by oxalate catalyzed photoelectro-fenton process using carbon nanotube-PTFE cathode. Desalination 258 (1–3), 112–119.
Khatoon, A., Uddin, M.K., Rao, R.A.K., 2018. Adsorptive remediation of Pb (II) from aqueous media using Schleichera oleosa bark. Environ. Technol. Innov. 11, 1–14.
Kurniawan, T.A., Chan, G.Y., Lo, W.-H., Babel, S., 2006. Physico–chemical treatment techniques for wastewater laden with heavy metals. Chem. Eng. J. 118 (1–2), 83–98.
Lertcumfu, N., Jaita, P., Thammarong, S., Lamkhao, S., Tandorn, S., Randorn, C., Tunkasiri, T., Rujijanagul, G., 2020. Influence of graphene oxide additive on physical, microstructure, adsorption, and photocatalytic properties of calcined kaolinite-based geopolymer ceramic composites. Colloids Surf. A 125080.
Li, Z., Kong, Y., Ge, Y., 2015. Synthesis of porous lignin xanthate resin for Pb^{2+} removal from aqueous solution. Chem. Eng. J. 270, 229–234.
Ma, S.-B., Ahn, K.-Y., Lee, E.-S., Oh, K.-H., Kim, K.-B., 2007. Synthesis and characterization of manganese dioxide spontaneously coated on carbon nanotubes. Carbon 45 (2), 375–382.
Madaeni, S., Mansourpanah, Y., 2003. COD Removal from concentrated wastewater using membranes. Filtr. Sep. 40 (6), 40–46.
Mahmoud, M.E., Osman, M.M., Hafez, O.F., Hegazi, A.H., Elmelegy, E., 2010. Removal and preconcentration of lead (II) and other heavy metals from water by alumina adsorbents developed by surface-adsorbed-dithizone. Desalination 251 (1–3), 123–130.
Marcano, D.C., Kosynkin, D.V., Berlin, J.M., Sinitskii, A., Sun, Z., Slesarev, A., Alemany, L.B., Lu, W., Tour, J.M., 2010. Improved synthesis of graphene oxide. ACS Nano 4 (8), 4806–4814.
Motlagh, P.Y., Khataee, A., Rad, T.S., Hassani, A., Joo, S.W., 2019. Fabrication of ZnFe-layered double hydroxides with graphene oxide for efficient visible light photocatalytic performance. J. Taiwan Inst. Chem. Eng. 101, 186–203.

Nejadshafiee, V., Islami, M.R., 2019. Adsorption capacity of heavy metal ions using sultone-modified magnetic activated carbon as a bio-adsorbent. Mater. Sci. Eng. C 101, 42–52.
Ngambia, A., Ifthikar, J., Shahib, I.I., Jawad, A., Shahzad, A., Zhao, M., Wang, J., Chen, Z., Chen, Z., 2019. Adsorptive purification of heavy metal contaminated wastewater with sewage sludge derived carbon-supported Mg (II) composite. Sci. Total Environ. 691, 306–321.
Rae, I.B., Pap, S., Svobodova, D., Gibb, S.W., 2019. Comparison of sustainable biosorbents and ion-exchange resins to remove Sr^{2+} from simulant nuclear wastewater: Batch, dynamic and mechanism studies. Sci. Total Environ. 650, 2411–2422.
Ramanayaka, S., Vithanage, M., Sarmah, A., An, T., Kim, K.-H., Ok, Y.S., 2019. Performance of metal–organic frameworks for the adsorptive removal of potentially toxic elements in a water system: a critical review. RSC Adv. 9 (59), 34359–34376.
Rao, M.M., Ramana, D., Seshaiah, K., Wang, M., Chien, S.C., 2009. Removal of some metal ions by activated carbon prepared from Phaseolus aureus hulls. J. Hazard. Mater. 166 (2–3), 1006–1013.
Rasoulpoor, K., Marjani, A.P., Nozad, E., 2020. Competitive chemisorption and physisorption processes of a walnut shell based semi-IPN bio-composite adsorbent for lead ion removal from water: Equilibrium, kinetic and thermodynamic studies. Environ. Technol. Innov. 20, 101133.
Safarpour, M., Vatanpour, V., Khataee, A., 2016. Preparation and characterization of graphene oxide/TiO_2 blended PES nanofiltration membrane with improved antifouling and separation performance. Desalination 393, 65–78.
Sun, J., Liu, L., Yang, F., 2020. A WO_3/PPy/ACF modified electrode in electrochemical system for simultaneous removal of heavy metal ion Cu^{2+} and organic acid. J. Hard Mater. 122534.
Tamez, C., Hernandez, R., Parsons, J., 2016. Removal of Cu (II) and Pb (II) from aqueous solution using engineered iron oxide nanoparticles. Microchem. J. 125, 97–104.
Thomas, K.V., Langford, K., 2007. Occurrence of pharmaceuticals in the aqueous environment. Compr. Anal. Chem. 50, 337–359.
Verma, M., Kumar, A., Singh, K.P., Kumar, R., Kumar, V., Srivastava, C.M., Rawat, V., Rao, G., Kumari, S., Sharma, P., 2020. Graphene oxide-manganese ferrite (GO-$MnFe_2O_4$) nanocomposite: One-pot hydrothermal synthesis and its use for adsorptive removal of Pb^{2+} ions from aqueous medium. J. Molecular Liquids 113769.
Wang, S., Ariyanto, E., 2007. Competitive adsorption of malachite green and pb ions on natural zeolite. J. Colloid Interface Sci. 314 (1), 25–31.
Wang, Y., Li, L., Luo, C., Wang, X., Duan, H., 2016. Removal of Pb^{2+} from water environment using a novel magnetic chitosan/graphene oxide imprinted Pb^{2+}. Int. J. Biiol. Macromol. 86, 505–511.
Wang, J., Wen, X., Yang, F., Cao, Z., Wang, S., Zhong, H., 2018. Preparation of a novel two-dimensional carbon material and enhancing Cu (II) ions removal by phytic acid. Envir. Earth Sci. 77 (12), 472.
Wu, Y., Guan, C.-Y., Griswold, N., Hou, Fang, X., Hu, A., Hu, Yu, C.-P., 2020b. Zero-valent iron-based technologies for removal of heavy metal (loid) s and organic pollutants from the aquatic environment: Recent advances and perspectives. J. Cleaner Prod. 123478.
Wu, W., Shi, Y., Liu, G., Fan, X., Yu, Y., 2020a. Recent development of graphene oxide based forward osmosis membrane for water treatment: A critical review. Desalination 491, 114452.
Yang, X., Zhang, X., Ma, Y., Huang, Y., Wang, Y., Chen, Y., 2009. Superparamagnetic graphene oxide–Fe_3O_4 nanoparticles hybrid for controlled targeted drug carriers. J. Mater. Chem. 19 (18), 2710–2714.
Yi, H., Liu, R., Chen, Z., Nie, B., 2020. Visible-light driven photodegradation on Ag nanoparticle-embedded fullerene (C60) heterostructural microcubes. Chemosphere 127355.
Zavareh, S., Zarei, M., Darvishi, F., Azizi, H., 2015. As (III) adsorption and antimicrobial properties of Cu–chitosan/alumina nanocomposite. Chem. Eng. J. 273, 610–621.
Zhang, B., Ma, Z., Yang, F., Liu, Y., Guo, M., 2017. Adsorption properties of ion recognition rice straw lignin on $PdCl_4^{2-}$: Equilibrium, kinetics and mechanism. Colloids Surf. A 514, 260–268.
Zhang, Z., Wang, T., Zhang, H., Liu, Y., Xing, B., 2020. Adsorption of Pb (II) and Cd (II) by magnetic activated carbon and its mechanism. Sci. Total Environ. 143910.
Zhao, T., Yao, Y., Wang, M., Chen, R., Yu, Y., Wu, F., Zhang, C., 2017b. Preparation of MnO_2-modified graphite sorbents from spent Li-ion batteries for the treatment of water contaminated by Lead, Cadmium, and Silver. ACS Appl. Mater. Interf. 9 (30), 25369–25376.
Zhao, D., Zhang, Q., Xuan, H., Chen, Y., Zhang, K., Feng, S., Alsaedi, A., Hayat, T., Chen, C., 2017a. EDTA Functionalized Fe_3O_4/graphene oxide for efficient removal of U (VI) from aqueous solutions. J. Colloid Interface Sci. 506, 300–307.
Zhou, Y., Meng, J., Zhang, M., Chen, S., He, B., Zhao, H., Li, Q., Zhang, S., Wang, T., 2019. Which type of pollutants need to be controlled with priority in wastewater treatment plants: Traditional or emerging pollutants?. Environ. Int. 131, 104982.